The Onset of Thermal Metamorphism in Enstatite Chondrites

Claire Bendersky

Mount Holyoke College

Advisors:

Professor M. Darby Dyar

Department of Astronomy, Mount Holyoke College

and

Professor M.K. Weisberg

Department of Physical Sciences, CUNY

Department of Earth and Planetary Sciences, AMNH

December 2006

ACKNOWLEDGEMENTS

First I would like to thank my parents, brother, and cousin Karen for their support and cheerleading. This project originally began as a research experience for undergraduates (REU) at the American Museum of Natural History in the Earth and Planetary Science department. The work atmosphere there was positive and encouraging. Dr. M. K. Weisberg served as my advisor. He was endlessly patient especially with explanations. More so he was inspiring. His enthusiasm for his work is infectious. Furthermore Dr. Denton Ebel, Joe Bosenberg, Dr. James Webster, Dr. Jon Friedrich, Dr. Charles Liu, Jacob Mey, Dr. Harold Connolly, Dr. Charlie Mandeville and Nannette Nicholson all served as wonderful role models and invaluable resources. I continued my research over the summer and through the fall semester, 2006, at Mount Holyoke

College under the guidance of Dr. M. Darby Dyar. I felt privilege to return to the lab where I began researching my freshman summer. I would very much like to thank Dr. M. Darby Dyar for all her support and advice over the years. I am happy to complete my undergraduate college career, with a research project that combines geology and astronomy, under her direction. Thanks to Marian Rice for her help with the SEM and the orange screen of death, Cindy Morrell for her smiles and quick wit, Catrina Hamilton and Mike Jercinovic. Thanks to Fred McGinness, Tom Burbine, and again Dr. M. Darby Dyar for sitting on my committee and reading this work. Finally I want to thank my friends who helped to keep me on my feet. Thanks to Michelle Thorne, Monica Liau, Brent Parris, Alexis Chapman, Diane Crenshaw, Lindsay Scannell, Madison Barkley, Patty Cobin, Corina Rusu, and Eli Sklute. A very special thank to AJ Carver. Thank you for pushing me to do my best.

CONTENTS

1 INTRODUCTION **1**

2 BACKGROUND **4**

3 SAMPLES & TECHNIQUES **13**

4 RESULTS **17**

4.1 MINERALOGY 18

4.2 DISTRIBUTION OF ELEMENTAL ABUNDANCES IN OLIVINE GRAINS 24

5 DISCUSSION **28**

6 CONCLUSION **39**

LIST OF FIGURES

2.1 Meteorite Tree 10

2.2 Plot of Chondrite Chemical Abundances Relative to the Sun . 11

2.3 Three isotope plot of Oxygen 12

4.1 Cr_2O_3 vs. FeO in Sahara 97096 Olivine 18

4.2 MnO vs. FeO in Sahara 97096 Olivine 19

4.3 CaO vs. FeO in Sahara 97096 Olivine 20

4.4 SEM Image of Yamato 691 21

4.5 SEM Image of Sahara 97096 22

4.6 SEM Image of Parsa 23

4.7 SEM Image of Kota Kota 24

4.8 SEM Image of Qingzhen 25

4.9 SEM Image of Linear Inclusions in Kota Kota 26

4.10 Histogram of Cr_2O_3 wt% for each sample. 27

5.1 Early stages of thermal metamorphism in O, CO, and E chondrites. 32

5.2 Early stages of thermal metamorphism in O and CO compared to Cr values for olivines with greater than 2 wt% FeO in E chondrites 36

LIST OF TABLES

3.1 Meteorite Thin Section Studied 14

4.1 Mean, standard deviation (σ), and Range of Olivine (wt%) of the compositional elements of Olivine 26

Abstract

Five E chondrites, Kota Kota, Parsa, Qingzhen, Sahara 97096, and Yamato 691, were studied to determine if Cr in olivine is useful as an indicator of thermal metamorphism. E chondrites are important because they are the only meteorites to have an oxygen isotopic composition similar to that of the Earth and Moon and thus may be analog material from which the Earth formed. They are also the most reduced chondrites. The redistribution of Cr in olivine during thermal metamorphism is studied with the petrographic microscope, scanning electron microscope (SEM) and electron microprobe (EMP). The conclusions of this study are 1) Cr in olivine is a good indicator of the early onset of thermal metamorphism in E chondrites, 2) olivine in E chondrites can be used to find the most primitive E chondrites, 3) the petrological types of five meteorites in this study are ordered from most to least primitive: Yamato 691, Sahara 97096, Parsa, Kota Kota, Qingzhen, and 4) during thermal metamorphism, Cr is redistributed into metal and sulfide phases in and around olivine grains.

CHAPTER 1

INTRODUCTION

The goal of this work is to identify which of five meteorites (Kota Kota, Parsa, Qingzhen, Sahara 97096, and Yamato 691) has changed the least chemically and mineralogically since being formed. All five samples are EH3 chondrites. Chondrites are meteorites with solar-like compositions. Enstatite (E) chondrites are the most reduced chondrites, which is why they are characterized by distinctive mineralogy, including a variety of unusual sulfide, metal, and nitride group minerals (Weisberg et al., 2006). E chondrites are categorized into two groups: those with high (EH) verse low (EL) metal Fe content. EL chondrites are low in metallic iron and contain Fe-rich silicate minerals (i.e. olivine, pyroxene, feldspar).

EH chondrites are rich in metallic iron, have Fe-poor silicate minerals, and are more reduced than ELs. EH chondrites are the most reduced of all chondrites.

Changes in the chemistry and mineralogy of meteorites are called metamorphism. Meteorites that have been the least metamorphosed contain the most information about the early solar system. Metamorphism, thermal or hydrous, is a secondary process that occurs after the formation of a meteorite. E chondrites are vital sources of information regarding conditions and processes in the early Solar System because they record information about conditions in the most reducing solar nebular environment known. Metamorphism veils the pristine, original, nature of the meteorite (Weisberg et al., 1994). To identify which EHs have been the least metamorphosed since formation is to find the EHs that contain the most information about the early Solar System.

The initial effects of thermal metamorphism in chondrites are recorded in the mineral olivine [(Mg, Fe)$_2$, SiO$_4$], a magnesium iron silicate. When olivine is heated, it may re-equilibrate to form other minerals such as chromite that are better hosts for Cr. As a result Cr becomes depleted in the olivine that is left behind (Leitch and Smith, 1982 and Grossman and Brearley, 2005). In order to determine which meteorites are least thermally metamorphosed, minor

element exsolutions in olivine grains are located using a scanning electron microscope (SEM) and the chemical compositions of the olivine grains are determined with an electron microprobe (EMP).

Grossman and Brearley (2005) created a new method that more precisely identifies the most pristine chondrites. They analyzed Fe-rich olivine in ordinary (O) and carbonaceous (C) chondrites and found that the amount of Cr in olivine, if the olivine has an FeO content greater than 2 wt%, can be correlated with the degree of thermal metamorphism experienced by the meteorite.

The purpose of this study is to understand the redistribution of Cr during thermal metamorphism and to determine if results for EH chondrite found with Grossman and Brearleys (2005) method, using olivine as an indicator of thermal metamorphism, can be applied to EH3 chondrites.

CHAPTER 2

BACKGROUND

All meteorites are considered either chondrites or achondrites (Figure 2.1). Achondrites are igneous rocks (melts, partial melts, melt residues) or breccias of igneous rock fragments from differentiated asteroids and planetary bodies (e.g. the Moon or Mars). Chondrites are meteorites with solar-like compositions (with the exception of volatile, light, elements like H and He) (Figure 2.2) and are derived from asteroids (and possibly comets) that did not experience planetary differentiation (Weisberg, 2006). The aggregate character of chondrites and their almost solar compositions set them apart from all other meteorites and all known terrestrial rocks (Hutchinson, 2004).

Chondrites are divided into three groups (Figure 2.1) based on whole-rock composition, O-isotopic composition, and petrologic characteristics including texture, mineralogy, and mineralogical compositions (Weisberg, 2006). Enstatite (E) chondrites have low Mg/Si ratios, are strongly reduced, and contain silicate minerals that are low in Fe. Elements such as Ca, Mn, Mg and K, which normally occur in silicates, are instead partitioned into sulfides. Carbonaceous (C) chondrites have low Mg/Si ratios and are strongly oxidized. Many are hydrated and most contain a significant Fe^{3+} in the mineral magnetite [Fe_3O_4]. Ordinary (O) chondrites lie between these extremes: they have intermediate Mg/Si ratios and contain significant amounts of both iron metal and oxidized iron in magnetite and silicates (Hutchinson, 2004).

The amount of depletion of volatile elements in chondritic groups is a function of temperature, which in turn is a function of distance from the Sun. The density and temperature of the gas and dust from which chondrites formed decreases with increasing solar distance, resulting in more highly reducing conditions closer to the Sun and more oxidizing conditions further away from the Sun (McSween, 2000). E chondrites are the most reduced chondrites known. Their high abundances of metal and the reduced state of iron in their minerals suggest they formed in the inner solar sys-

tem close to the Sun. EH chondrites are more reduced than EL chondrites, meaning that they are the most reduced E chondrites (and hence chondrites) and that they formed closer to the sun then EL chondrites.

E chondrites share a unique relationship with the Earth and Moon; they all posses a particular oxygen isotope signature that is represented by the terrestrial fractionation line (TF) on the tree oxygen isotope plot (Figure 2.3). Oxygen is the only element known to vary in isotopic composition between different chondrites, if cosmogeneic and radiogenetic effects and fractionation observed in highly volatile rare gases are ignored (Wasson, 1985). Each chondrite group occupies a specific region on the three-isotope plot for oxygen (Figure 2.3). E chondrites are the only chondrites to fall on the TF line (Figure 2.1), which may indicate that they are analogues of the precursor materials that formed the Earth and Moon (Weisberg et al., 2006). E chondrites formed under highly reducing nebular conditions, as recorded by their mineralogy and mineral chemistry (Keil, 1968). They contain Fe-poor silicate minerals, Si-bearing metal, and elements that are generally bonded to silicon in most meteorite groups (Mn, Mg, Ca, Na, and K) that can behave as sulfur bonding elements. In E chondrites enstatite [$MgSiO_3$] is the major silicate mineral in chondrules.

Each chondrite is assigned a number according to petrologic type. Petrologic type is based on the degree of hydrous/thermal metamorphism expressed on a scale from 1 to 7. Petrologic type expresses the degree of metamorphism experienced by a chondrite. A one- or two- letter symbol for a chondrite group is combined with the number of a petrologic type as a convenient shorthand designation of the chondritic-petroloic class (Hutchinson, 2004). Type 3 is thought to represent the most pristine materials, type 4 to 6 indicate increasing degree of thermal metamorphism, and 2 to 1 represent increasing degree of hydrous alteration in chondrites (Weisberg et al., 2006). One of the defining criteria for type 3 enstatite chondrites is the presence of olivine. Olivine is completely absent in the higher petrologic types: E4, E5, and E6 chondrites (Weisberg, 2005). Olivine is a minor mineral in E chondrites and as their name suggests, enstatite is the major mineral. Sears et al. (1980) showed that sensitivity to induced thermal luminescence (TL) can be used to define ten subtypes (3.0 3.9) in O chondrites and some C chondrites of petrologic type 3 (Hutchinson, 2004).

It is important to fully characterize the lowest end of the metamorphic sequence displayed by chondrites for several reasons. Ideally, type 3.0 chondrites represent material unchanged by metamorphic processes on asteroids and therefore are the most suitable

for the study of nebular processes. It is important to determine if such meteorites exist in collections, and to establish accurate and quantitative methods of identifying them. For meteorites slightly affected by heating (types 3.1 and 3.2), the extent of the resultant changes must be understood in order to see through the veil of metamorphism and learn about the early solar system. Careful comparison of the geochemical and petrological properties of types 3.0, 3.1, and 3.2 chondrites can therefore be used to gain a more complete understanding of a variety of early asteroidal processes, including thermal processing and aqueous alteration (Grossman and Brearley, 2005).

Grossman and Brearley (2005) observed that the distribution of Cr in silicates appeared to be different in type 3.0 chondrites relative to higher petrologic types (3.1 and greater). Previous work (Dodd 1973; Ashworth 1979; McCoy et al. 1991; Johnson and Prinz 1991; Dehart et al. 1992; Jones and Lofgren 1993) indicated that the Cr content of olivine might be related to metamorphic grade. This phenomenon had never been studied in detail. Grossman and Brearley (2005) found that Type I (Mg-rich) chondrules appear to have low Cr contents regardless of petrologic type. Furthermore, below 2 wt% FeO, Cr_2O_3 and FeO are correlated and are apparently controlled by the same process. At low FeO con-

tents, MnO also correlates and CaO anticorrelates with FeO in olivine, implying a volatility control of all minor elements, including Cr. Volatility control refers to a condition in the formation of these chondrites (Hutchinson, 2004). In the latter quote Grossman and Brearley (2005) state the abundance and distribution of Cr_2O_3 does not indicate the degree of thermal metamorphism in O and CO chondrites. Instead, volatility, a part of the formation process, controlled the abundance of volatile oxides (Cr_2O_3, MnO, and CaO) in olivine.

Grossman and Brearley (2005) did not consider Mg-rich olivine because of the correlation between FeO and Cr_2O_3, FeO and MnO, and the anticorrelation between FeO and CaO. They support their decision with "literature from Scott and Jones (1990), Jones (unpublished data), and Brearley and Jones (1998)...[that] suggest that the 2-3 wt% FeO cutoff is also reasonable for this [CO] chondrite group." Mg-rich olivine is prevalent in E chondrites; while Fe-rich olivine is almost non-existent. Accordingly the present study applies the Grossman and Brearley (2005) method to Mg-rich olivine in E chondrites.

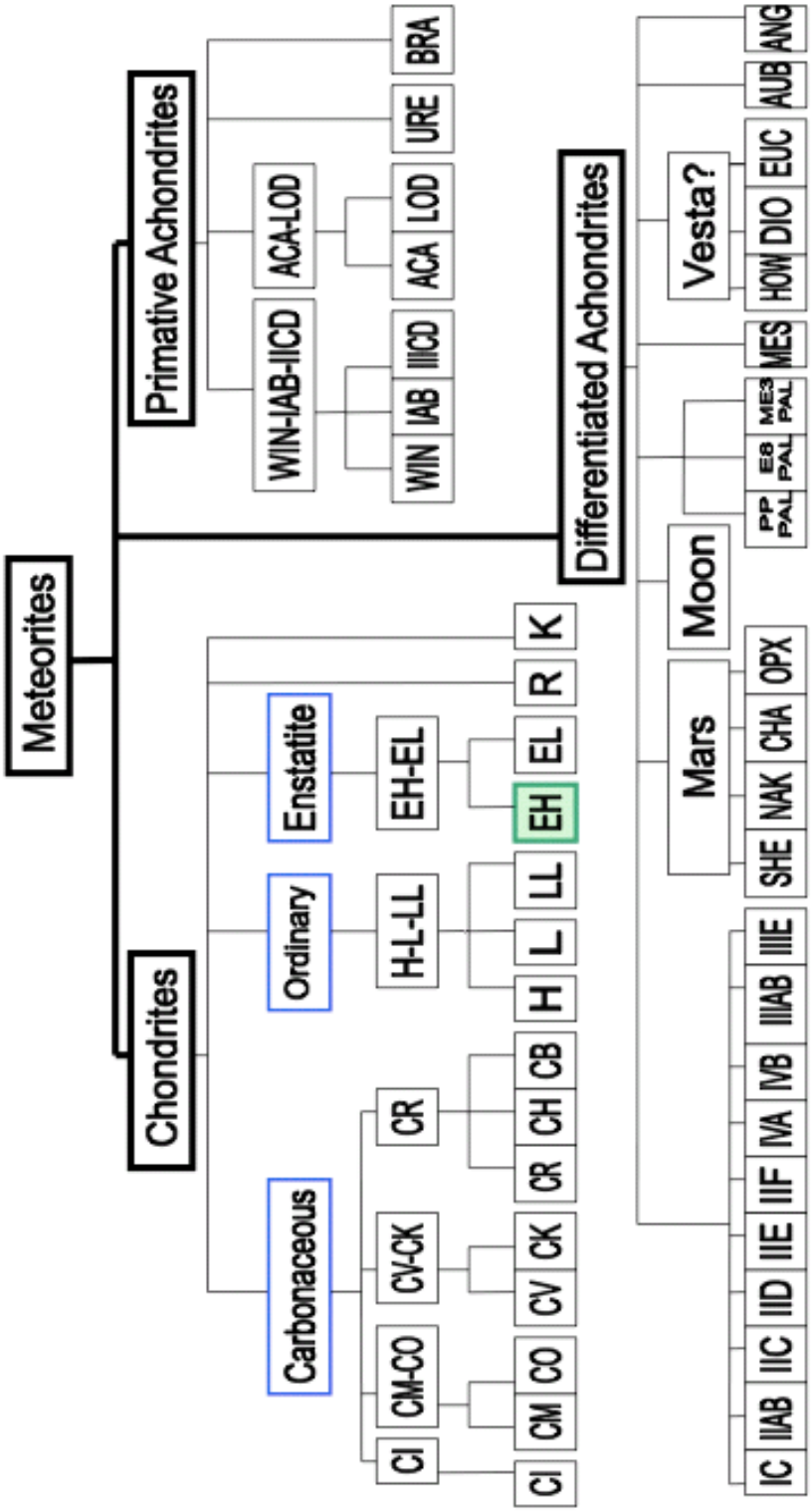

Figure 2.1: Meteorites are subdivided into two groups: chondrites and achondrites. The bolded boxes represent the primary types of chondrites. This study focuses on chondrites, particularly EH chondrites. Image source: This image was adapted from Weisberg et al. (2006).

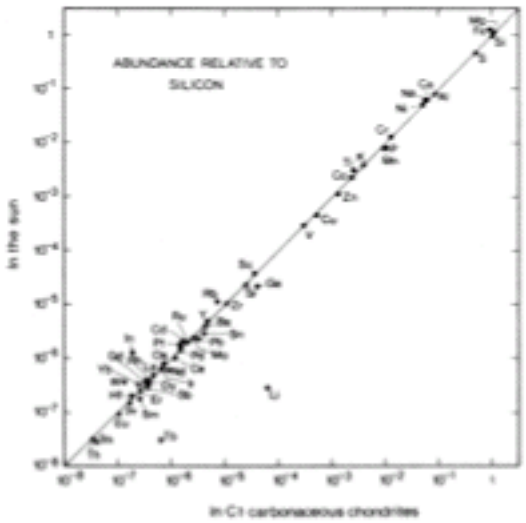

Figure 2.2: Chemical abundances measured in CI chondrites, relative to Si, are compared to their relative abundances found in the Sun. The diagonal line represents equal abundances found in the Sun and in CI chondrites (Landstreet, 2000). Source: Grevesse N. and Sauvel AJ., 1998

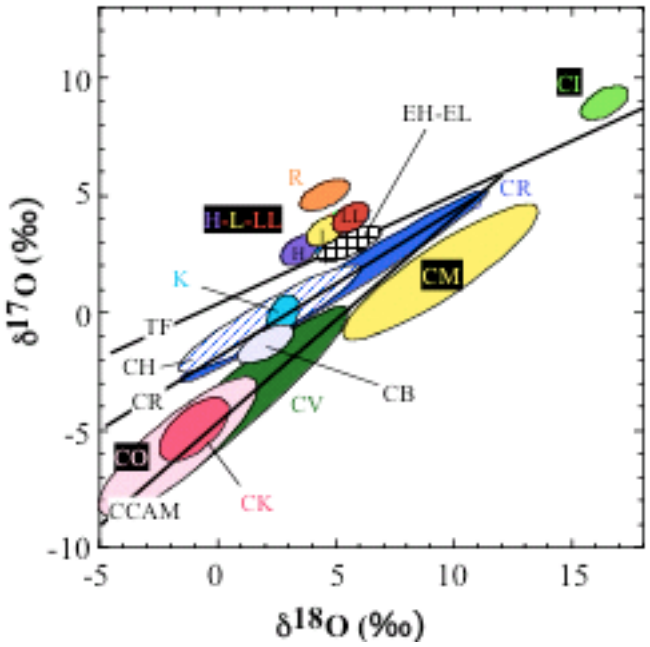

Figure 2.3: Three isotope plot for oxygen. All areas labeled by a chondritic type designated by a two letter combination. Those labels beginning with C are C chondrites. Ordinary chondrites are labeled H, L, and LL. E chondrites are labeled EH and EL. E chondrites are the only chondrites to fall on the T-F line. This diagram is called three isotope plot for oxygen because the axes labels δ^{18}O and δ^{17}O represent the ratio of ^{18}O/^{16}O and ^{17}O/^{16}O respectively. Oxygen has three isotopes: ^{16}O is by far the most abundant, ^{18}O is less so and ^{17}O is rare. On a three-isotope plot this is illustrated by the terrestrial fracationation line (TF). To a close approximation the oxygen isotopic ratios of all Earth material plot on the line that has a slope close to 1/2; 0.52., to be precise (Hutchinson, 2000). Image source: Weisberg, 2006.

CHAPTER 3

SAMPLES & TECHNIQUES

Polished thin sections Kota Kota AMNH 4075-1, Parsa AMNH 4549-1, Qingzhen AMNH 4653-1, Sahara 97096 AMNH 4940-1 and Yamato 691 AMNH 4878-1B were used for this study.

Using the petrologic microscope, olivine grains from chondrules and fragments were identified. At least 20 were chosen in Kota Kota, 30 in Parsa, 15 in Qingzhen, 45 in Sahara 97096 and 20 Yamato 691. Site locations for subsequent analyses were recorded on X-ray, BSE, and reflected light maps. Under cross-polarized light, olivine appears bright pink and blue. Olivine stands out against enstatite, which has low birefringence. Enstatite appears

NAME	KEY	SECTION[a]	CLASS	REF[b]
Kota Kota	Kota Kota	AMNH 4075-1	EH3	Pr84
Parsa	Parsa	AMNH 4549-1	EH3	Bh75
Qingzhen	Qinhgzhen	AMNH 4653-1	EH3	Wa77
Sahara 97096	Sahara 970976	AMNH 4940-1	EH3	We98
Yamato 691	Y 691	AMNH 4878-1B	EH3	Ma73

Table 3.1: The meteorites and polished thins sections analyzed for this work. [a] Loaning Institution: AMNH = American Museum of Natural History [b] Petrologic type determined by Pr84 = Prinz et al (1985); Bh75 = Bhandari H. et al (1975); Wa77 = Wang D. and Xie. X (1977); We98 = Weisberg M. K. et al (1998); Ma73 = Shima et al (1973).

grey under crossed polarized light. Dr. Ebel compiled X-ray maps of Kota Kota and Sahara 97096. Dr. Weisberg compiled a reflected light photo mosaic of Kota Kota. Ms. Bendersky compiled BSE maps of Parsa, Qingzhen, and Yamato 691.

The Princeton Gamma Tech (PGT) energy dispersive spectroscopy (EDS) system and backscatter electron (BSE) detector of the Hitachi S4700 field emission scanning electron microscope (FESEM) at the American Museum of Natural History (AMNH) were used to qualitatively analyze and image olivine sites in the sections of Kota Kota and Sahara 97096. A total of 6 sites (4 from Kota Kota and 2 from Sahara 97096) were studied in detail and 23 images were acquired. The EDAX Phoenix Pro Energy Dispersive Spectrometer EDS system and backscatter electron (BSE) detector of the Quanta 200 environmental scanning electron microscope

(ESEM) at Mount Holyoke College were used to qualitatively analyze and image olivine sites in the sections of Parsa, Qingzhen, and Yamato 691. A total of 23 sites (10 from Parsa, 8 from Qingzhen, and 5 from Yamato 691) were studied in detail and 27 images were recorded. The voltage was set to 20.0 kV and the current to 20 μA. The BSE detector was used to image Cr-rich inclusions in olivine and document Cr concentrations. The EDS verified the elements present in the olivine grains of interest. It was used to confirm that olivine grains were in fact olivine, and to determine the presence and location of Cr-rich inclusions within olivine crystals.

The Cameca SX100 electron microprobe (EMP) at the AMNH was used to obtain elemental abundances of olivine grains in Kota Kota (19 grains, 39 analyses), and Sahara 97096 (35 grains, 69 analyses). The excitation voltage was set to 20.0 kV and the sample current to 15μA. Olivine grains were analyzed by point (1μm) bean electron microscope analysis. Cr was calculated as Cr_2O_3, although the actual oxidation state is unknown; both Cr^{2+} and Cr^{3+} may be present (Sutton et al., 1996).

The Cameca SX50 EMP at the University of Massachusetts Amherst was used to obtain elemental abundances of olivine grains in Parsa (25 grains, 149 analyses), Qingzhen (11 grains, 66 analyses), and Yamato 691 (16 grains, 72 analyses). The excitation

voltage was set to 20.0 kV and the sample current to 15μA. Olivine grains were analyzed by point (1μm) bean electron microscope analysis.

CHAPTER 4

RESULTS

To determine that the redistribution of Cr is due to thermal metamorphism, not volatility, the weight percent of minor elements is plotted against the weight percent of FeO. Below 2 wt% FeO: Cr_2O_3 and FeO are not strongly correlated, $R^2 \approx 0.27$ (Figure 4.1); MnO is uniformly enriched around 0.13% (Figure 4.2); and CaO is uniformly enriched 0.14% (Figure 4.3). To facilitate comparison figures 4.1, 4.2, and 4.3 are all plotted on the same scale. Furthermore a labeled line at 2 wt% FeO is included in these figures as a visual aid, heightening correlations below 2 wt% FeO.

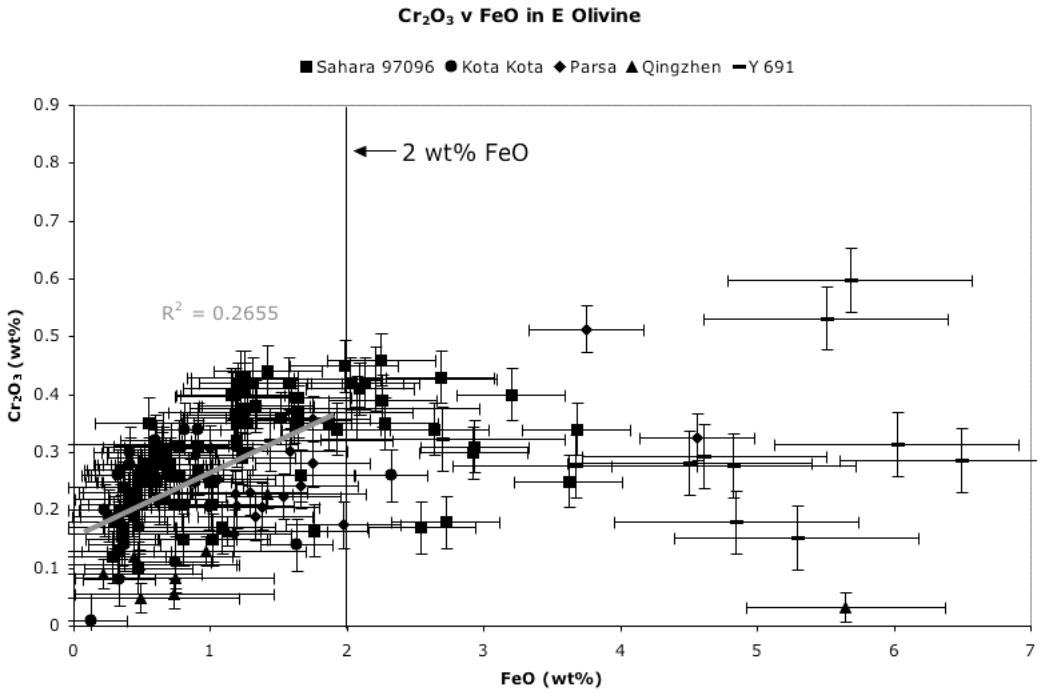

Figure 4.1: Below 2 wt% FeO, Cr_2O_3 shows a weak positive relationship, $R^2 \approx 0.27$

4.1 MINERALOGY

Inclusion distribution is observed to vary between meteorites. Figures 4.4, 4.5, 4.6, 4.7, 4.8, and 4.9, are of regions of interest centered on representative olivine grains of each meteoritic thin section. They are backscatter electron (BSE) images taken with the scanning electron microscope (SEM). Olivine is darker than enstatite in BSE images because olivine has a higher Mg to Si ratio than enstatite (2:1 and 1:1 respectively).

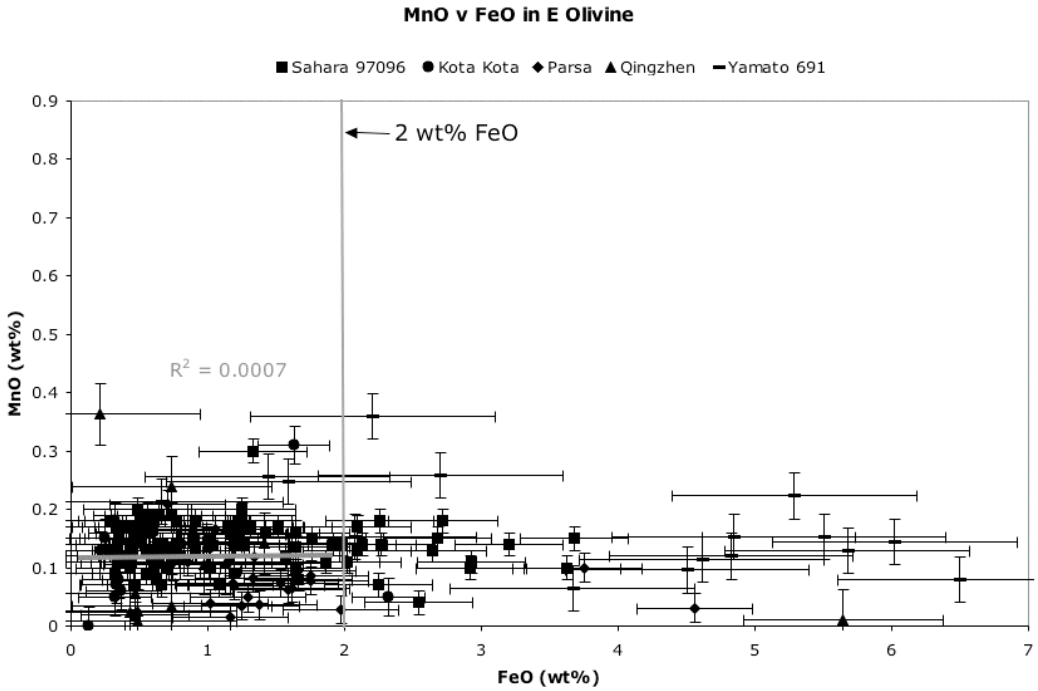

Figure 4.2: MnO is uniformly enriched ∼0.14 wt%. Below 2 wt% FeO, MnO and FeO display no relationship.

Yamato 691 has the greatest mean Cr_2O_3 wt% in olivine, 0.333 wt% (Table 4.1 and Figure 4.10). A few streaks are found through the olivine grain. At a magnification of 3339x, the streaks are visable but the constituents of each streak are not accurately measurable. Constituents are likely ∼0.20μm. No large inclusion blobs are seen in or around the olivine grains. Large parts of the grain are void of inclusions (Figure 4.4).

Sahara 97096 has the next greatest mean Cr_2O_3 wt% in olivine, 0.280 wt%, followed closely by Parsa with 0.276 wt% (Table 4.1 and

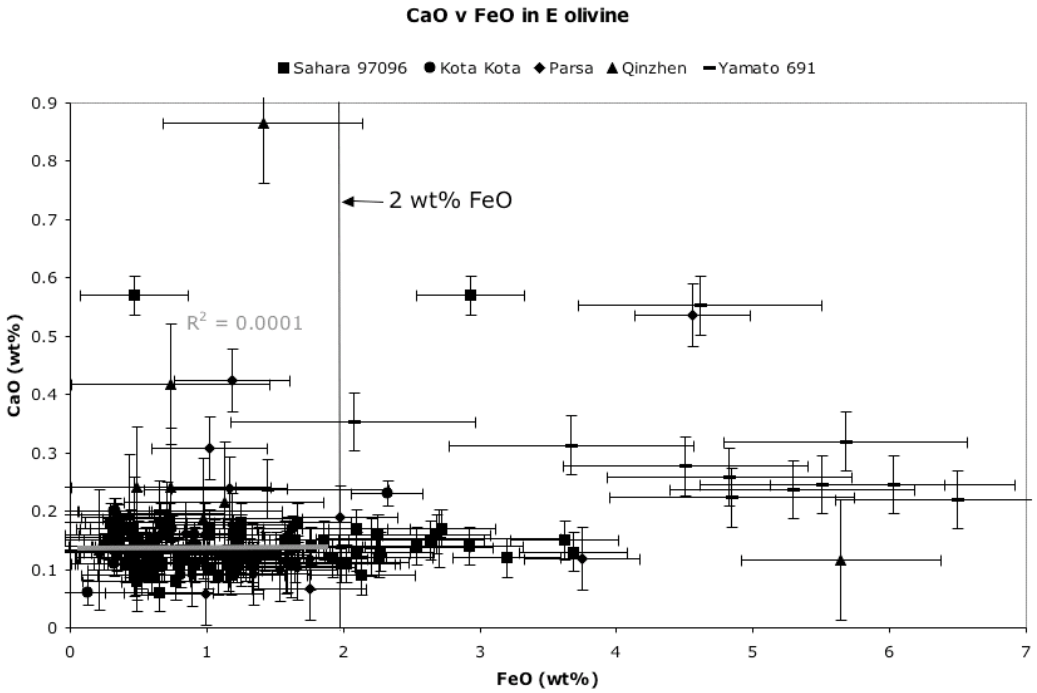

Figure 4.3: CaO is uniformly enriched ∼0.13 wt%. Below 2 wt% FeO, CaO and FeO display no relationship.

Figure 4.10). Both samples contain inclusions, large blobs in Parsa (Figure 4.6), streaks and perimeter blobs in Sahara 97096 (Figure 4.5). Between the streaks and isolated blobs, most of the crystal, the olivine grain is void of inclusions. In Sahara 97096, inclusions are found around the olivine grain and in streaks across the olivine grain (Figure 4.5). The nearly linear form of the streaks implies a control on the exsolution process. The exsolution blobs around the olivine grain measure ∼1.0μm or greater. Olivine grains in Parsa show few inclusions. The inclusions tend to surround the grains. A few larger inclusions blobs, ∼4.0μm, are located towards the center

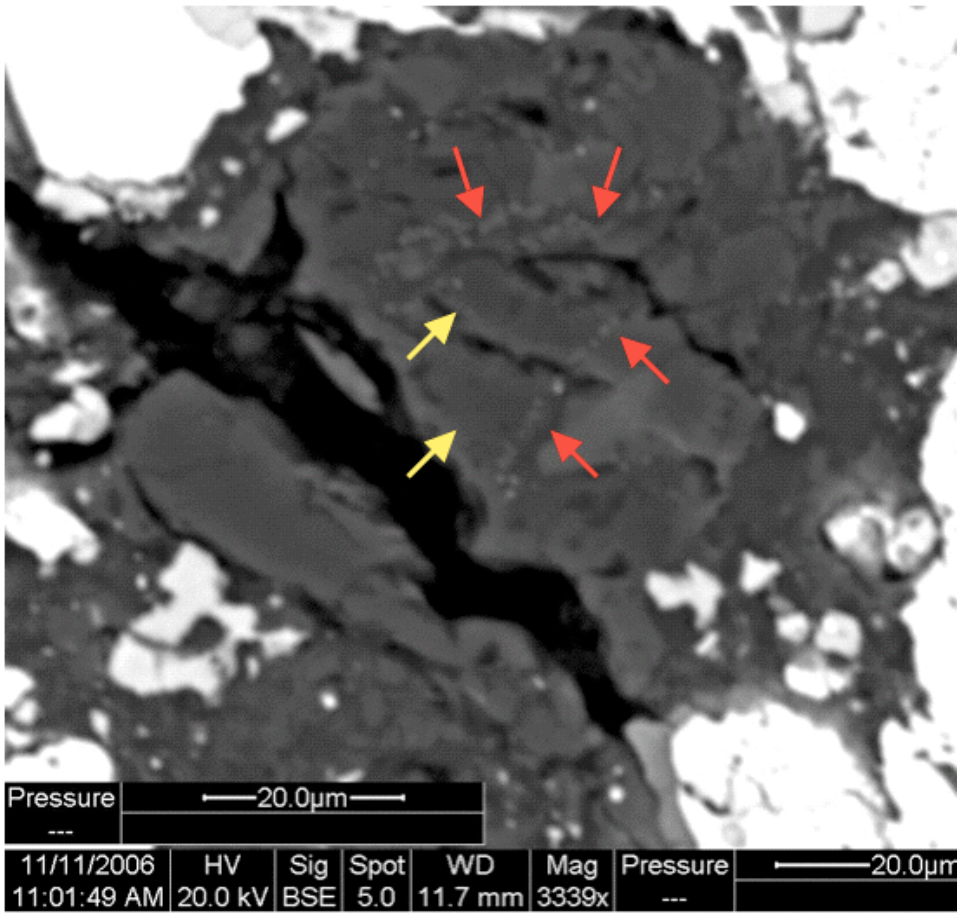

Figure 4.4: In Yamato 691exolution is only seen in the olivine grains (red arrows) and most of the olivine grain is void of inclusions (yellow arrows).

of the olivine grain (Figure 4.6). Between the streak and isolated blobs, most of the crystal, the olivine grains are void of inclusions.

Kota Kota contains 0.200 wt% Cr_2O_3 and displays many inclusions (Table 4.1 and Figure 4.10). The grains are mottled in appearance. Inclusions are abundant around the olivine grain and in

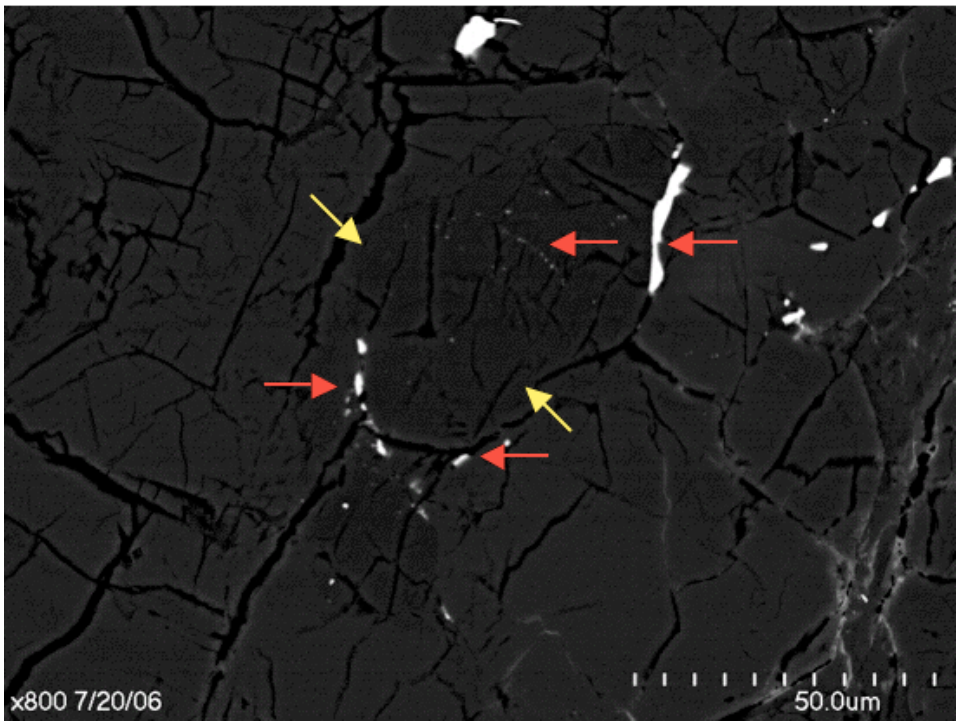

Figure 4.5: In Sahara 97096 inclusions are abundant around the olivine grain and in streaks (red arrows). The areas between streak and isolated blobs is void of inclusions (yellow arrows)

the central areas. Exsolution features around the olivine grain complement the shape of the olivine grain borders half of the olivine grain perimeter, and are as large as ∼20.0μm. The olivine grain has little space void of inclusions (Figure 4.7).

Qingzhen has the lowest mean Cr_2O_3 0.106 wt%, of the five meteorites studied (Table 4.1 and Figure 4.10). The grains are mottled. Large inclusions are found around the perimeter of the olivine grain and some within the grain (Figure 4.8).

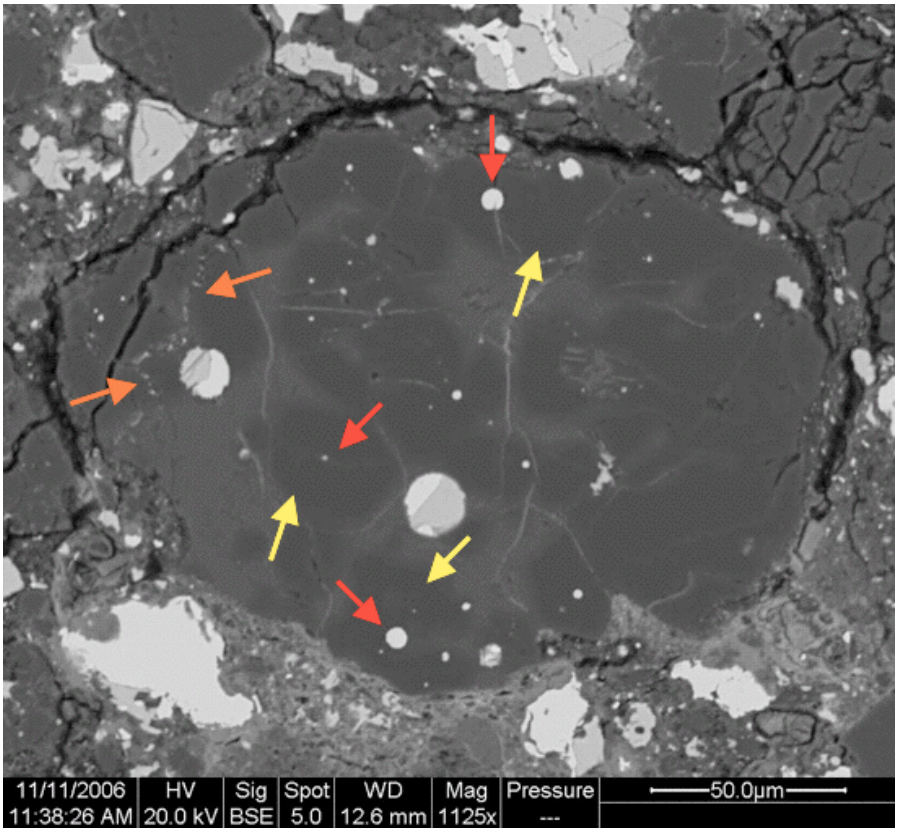

Figure 4.6: Olivine grains in Parsa show few inclusions. Inclusions surround olivine grains (orange arrows) and form a few larger blobs towards the center of the olivine grain (red arrow). The inner rim areas of the olivine grains are void of inclusions (yellow arrows).

Inclusions within the olivine grains are nearly linear (Figures 4.4, 4.5, and 4.9). At lower magnifications, less than 2500x, this might be difficult to see (Figure 4.7). At higher magnifications, greater than 2500x, one can observe that the inclusions are nearly linear (Figure 4.9). Larger blobby inclusions are commonly located on the perimeter, and sometimes within, the olivine grains (Figures

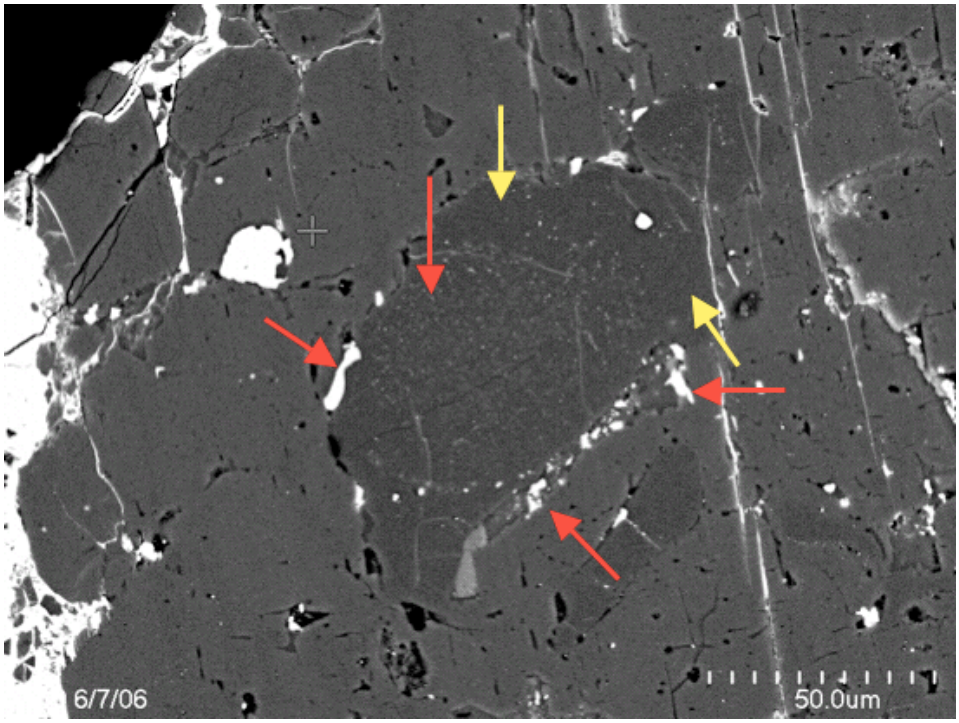

Figure 4.7: An olivine grain (dark grey area) in Kota Kota is mottled in appearance. Inclusions are found around and in the center of the olivine (red arrows). There are zones void of inclusions.

4.5, 4.6, 4.7, 4.8, and 4.9). All inclusions are metal and sulfide and a number of them have high quantities of minor elements Cr, Mn, and Ca. All inclusions are interpreted to have exsolved from the olivine crystal structure.

4.2 DISTRIBUTION OF ELEMENTAL ABUNDANCES IN OLIVINE GRAINS

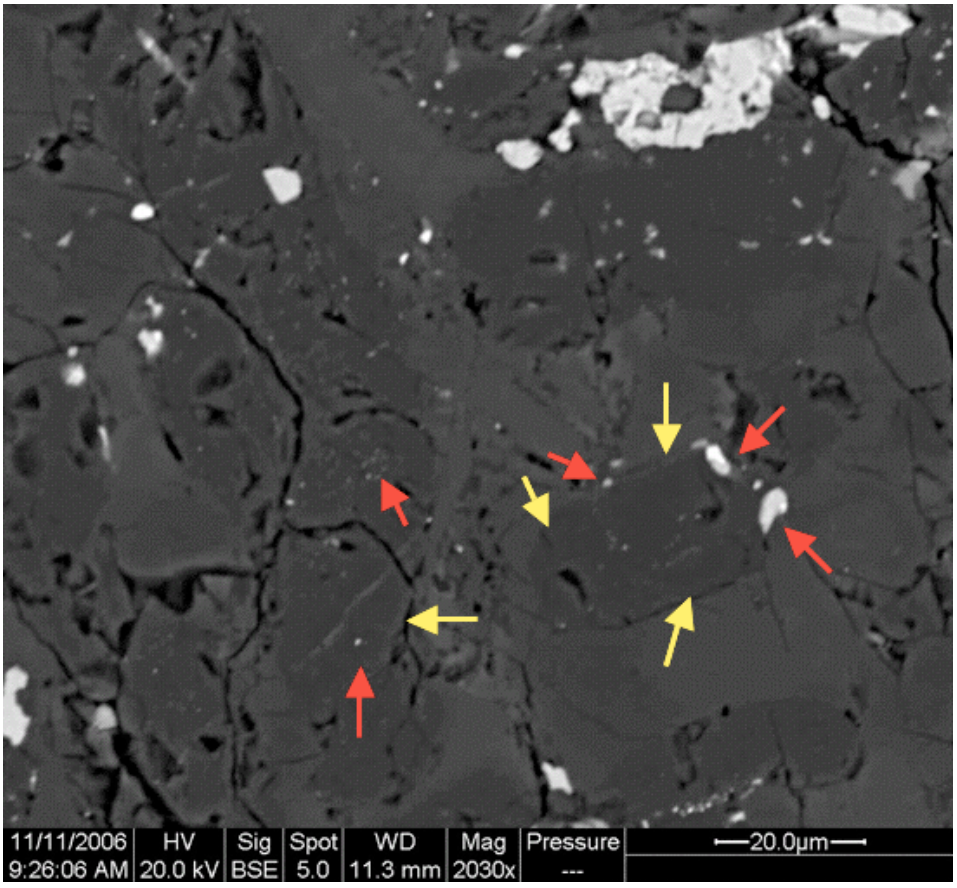

Figure 4.8: Inclusions are isolated around and with in the olivine grains (red arrows). B them olivine grains are void of exsolution features (yellow arrows).

The mean, range, and standard deviation of the compositional elements of olivine, for each sample, are listed in Table 4.1. All measurements of olivine composition were made on areas of olivine grains that had no visible inclusions (at all instrumentally possible magnifications) and that had spectra consistent with pure olivine. Additional data for Sahara 97096 were acquired from unpublished research by Weisberg.

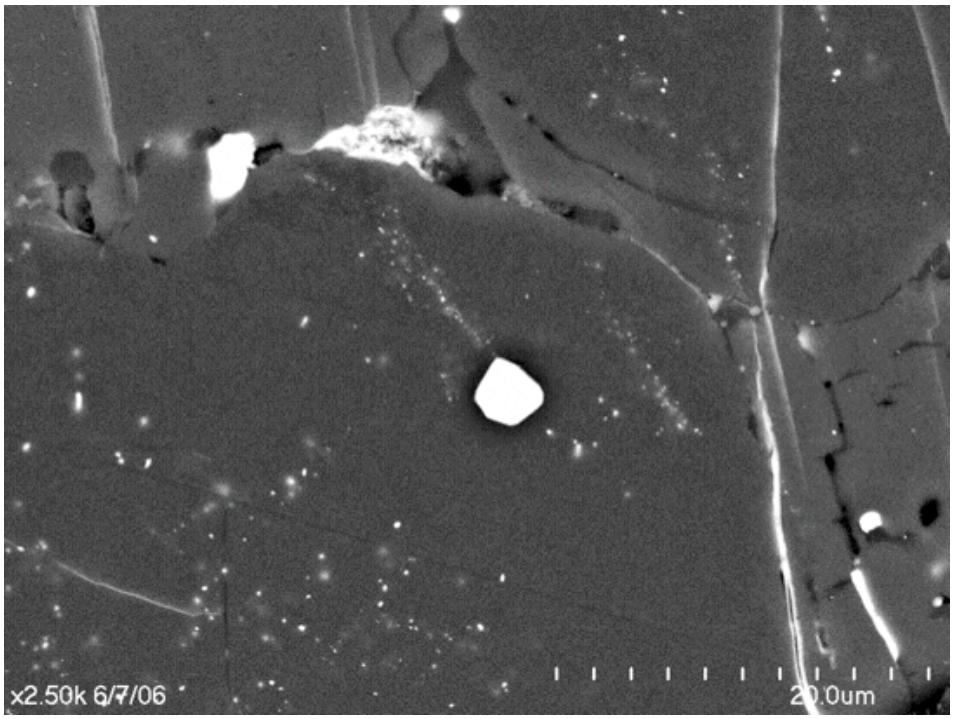

Figure 4.9: Linear inclusions in Kota Kota.

		SiO_2	MgO	CaO	TiO_2	Cr_2O_3*	MnO	FeO	NiO
Kota Kota	Mean	42.840	56.170	0.150	bd	0.200	0.120	0.530	bd
	σ	0.600	0.630	0.040	bd	0.100	0.060	0.360	bd
	Range	43.7-40.7	57.2-53.4	0.23-0.06	bd	.34-0	0.31-0	2.32-0.13	bd
SAH97096	Mean	42.270	55.920	0.140	bd	0.280	0.140	1.180	bd
	σ	0.550	0.860	0.070	bd	0.100	0.040	0.840	bd
	Range	43.7-40.8	58.3-51.5	0.57-0.06	bd	0.46-0.01	0.30-0.02	3.68-0.18	bd
Parsa	Mean	41.448	57.155	0.164	bd	0.276	0.088	1.159	bd
	σ	0.611	0.845	0.111	bd	0.086	0.050	0.861	bd
	Range	42.7-40.3	58.2-54.5	0.54-0.06	bd	0.513-0.15	0.21-0.00	4.6-0.71	bd
Qinqzhen	Mean	41.413	56.159	0.264	bd	0.106	0.102	1.155	bd
	σ	0.923	1.665	0.216	bd	0.056	0.111	1.529	bd
	Range	42.4-39.7	58.0-53.1	0.87-0.12	bd	0.23-0.00	0.36-0.00	5.6-0.21	bd
Y 691	Mean	41.566	54.334	0.255	bd	0.333	0.173	3.881	bd
	σ	0.666	1.550	0.102	bd	0.113	0.080	1.846	bd
	Range	42.9-40.5	56.7-52.3	0.55-0.11	bd	0.60-0.15	0.36-0.00	6.5-0.66	bd

Table 4.1: Mean, σ, and range (wt%) of the composition elements of olivine. *Cr is listed here as Cr_2O_3 however it represents Cr^{+2} and Cr^{+3}. bd stands for below detection.

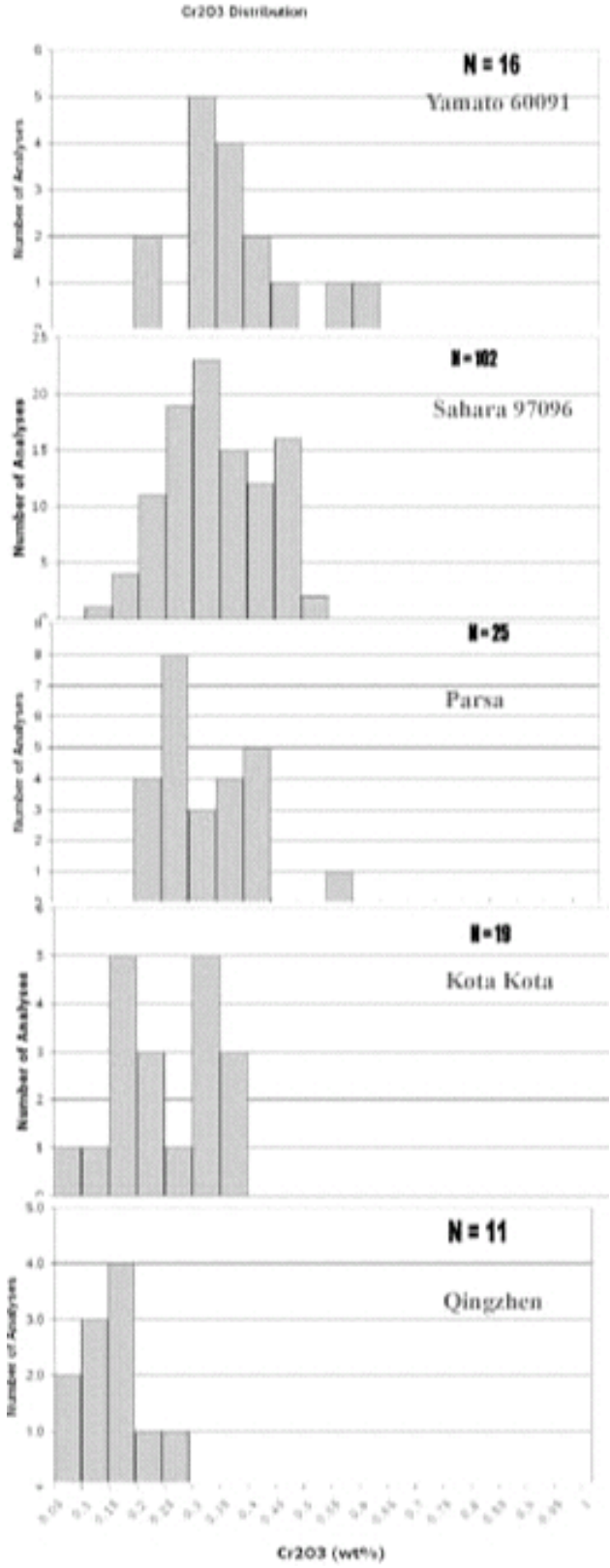

Figure 4.10: Histogram of Cr_2O_3 wt% for each sample.

CHAPTER 5

DISCUSSION

Petrologic type is expressed on a scale from 1 to 7 based on chemical and petrologic parameters that vary with degree of hydrous/thermal metamorphism. As metamorphic grade increases, diffusion homogenizes Fe and Mg in olivine; small grains are affected first. Heating results in progressive loss of volatiles (Sears et al., 1980). Grossman and Brearley (2005) developed a method that differentiates petrologic types of chondrites that experienced minor degrees of thermal metamorphism, "enabling the assignment of accurate petrologic types to highly unequilibrated" ordinary (O) and carbonaceous (C) chondrites. Grossman and Brearley (2005) found that Cr_2O_3 abundance and distribution in Fe-rich olivine var-

ied according to the degree of thermal metamorphism in O and C chondrites. "The measurement of Cr_2O_3 in ferroan olivine is one of the most straight forward [measurements] to make and is nearly unaffected by processes such as aqueous alteration and terrestrial weathering" (Grossman and Brearley, 2005).

In extending Grossman and Brearleys (2005) method to enstatite (E) chondrites, this study needs to address the following: Grossman and Brearley used only olivine with FeO contents above 2 wt% and olivine of this composition is extremely rare in the E chondrites.

This study finds it valid to apply the Grossman and Brearley (2005) method to olivine with less than 2 wt% FeO in E chondrites. Grossman and Brearley (2005) excluded low FeO olivine in O and C chondrites because they found that FeO correlated with each Cr_2O_3, MnO, and CaO. They concluded that these correlations are due primarily to volatility control during chondrule formation and are not the result of metamorphism. In this study of E chondrites, FeO and Cr_2O_3 are weakly correlated in low FeO olivine (Figure 4.1). There is no significant relationship between FeO with each MnO and CaO. MnO does not correlate nor does CaO anticorrelate with FeO in low FeO olivine (Figure 4.2 and Figure 4.3, respectively). The absence of these correlations indicates

the redistribution of Cr is due to metamorphism and not volatility.

The inclusions in olivine are most likely the result of remobilization of minor elements during thermal metamorphism. Exsolution features are Fe-rich metal or sulfide-rich metal or Fe-sulfide-rich and are often combined with minor elements from olivine (such as Cr). The metal and sulfide inclusions contain variable amounts of Cr which most likely exsolved from the olivine. Inclusions within the olivine grains may appear randomly distributed (Figures 4.7 and 4.8) but on a smaller scale they are arranged in nearly linear patterns (Figures 4.4, 4.5, 4.6, and 4.9). Nearly linear patterns of exsolution features suggest structural control on the exsolution process. It is possible that crystal faces control this structure. Crystal faces may provide zones of weakness that are easier to exsolve along. Larger exsolution features grow around the circumference of an olivine grain (Figures 4.5, 4.7, and 4.8) possibly because a larger zone of weakness exists between the olivine crystal face and the adjacent enstatite crystal face.

Grossman and Brearley (2005) graphed their samples on a plot of standard deviation versus the mean wt% of Cr_2O_3 in olivine. They drew a line to fit the O chondrite samples and the CO chondrite samples. Grossman and Brearley split the O chondrite line into five regions of petrologic type from 3.00 to 3.20 in increments

of 0.05 based on the distribution characteristics of Cr in the olivine of the meteorites. The CO chondrite line is shaped similarly to the O chondrite line and is shifted down and leftward in comparison to the O chondrite line. Despite similar shapes of the O chondrite and CO chondrite lines, the CO chondrite line is not split into regions of petrologic type because a standard CO meteorite needed to calibrate the divisions does not exist. Nevertheless, Grossman and Brearley conclude the most primitive CO meteorite is located the furthest to the right on the CO line i.e. the CO with the highest mean Cr_2O_3 wt%.

On the Grossman and Brearley graph below, the E chondrites of this study are plotted. The values of E chondrites are below those of the O chondrites and are located near the values of the CO chondrites. A line drawn through the data of E chondrites does not turn over because for these five samples Cr_2O_3 wt% is directly correlated with the distribution of Cr_2O_3. A trend similar to O and CO chondrites, with a turn over, might still be possible and can be determined with more samples.

The five samples are discussed in order of descending Cr_2O_3 wt%. Yamato 691 contains the most Cr_2O_3 with 0.33 wt%, the most MnO with 0.17 wt%, the most FeO with 3.88 wt%, and the second most CaO with 0.26 wt% (Table 4.1). No large exsolution

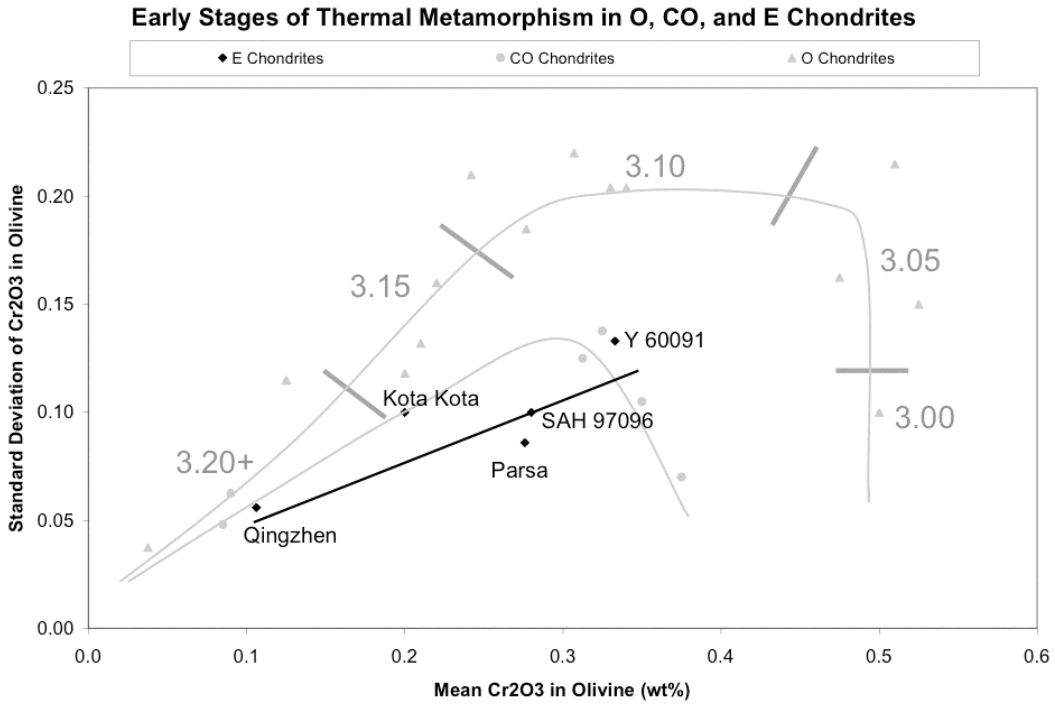

Figure 5.1: Early stages of thermal metamorphism in O, CO, and E chondrites.

features are seen around the olivine grain. Linear exsolution features, streaks, are seen within the grain (Figure 4.4). At 3339x magnification, the streaks are viable but the constituents of each streak are not accurately measurable (Figure 4.4). Constituents of each streak are roughly 0.20μm. Areas between the linear features in the olivine grain appear to be void of exsolution (Figure 4.4). Yamato 691 has the highest standard deviation, the most varied mean value, of Cr_2O_3 with 0.113 wt %(Table 4.1 and Figure 4.10). Exsolution occurs within in the olivine grain of Yamato 691.

Exsolution is absent on the perimeter of olivine grain. Since this meteorite contains the most Cr_2O_3 its the most primitive, meaning Yamato 691 has experienced less thermal metamorphism than Sahara 97096, Parsa, Kota Kota, and Qingzhen. Earlier stages of thermal metamorphism generate exsolution within the olivine grains. The large standard deviation may indicate that at earlier stages of thermal metamorphism olivine grains are depleted of minor elements at varying rates. These varying rates would then probably correspond to surface area to volume ratio.

Sahara 97096 has the second highest Cr_2O_3 content with 0.280 wt% and a high standard deviation of Cr_2O_3 with 0.100 wt% (Table 4.1 and Figure 4.10). Exsolution features on the perimeter of the olivine grains are larger than those within the olivine grain and complement the shape of the olivine grain. A few streaks of exsolution cross the olivine grain and a few isolated blobs of exsolution are visible (Figure 4.5). The constituents of the streaks and the isolated blobs in Sahara 97096 are bigger than the constituents of the streaks in Yamato 691. Those in Yamato 691 are $\sim$0.20μm. The largest exsolution blobs in Sahara 97096 are at least 1.0μm. Between the streaks and the isolated blobs the olivine grain, an area describing most of the crystal, appears to be void of exsolution. Sahara 97096 has experienced more thermal metamorphism

than Yamato 691. This higher degree of thermal metamorphism initiates exsolution around the olivine grain and larger exsolution blobs within the olivine grain.

Parsa has the third highest Cr_2O_3 content with 0.276 wt% and a moderate standard deviation of Cr_2O_3 with 0.086 wt% (Table 4.1 and Figure 4.10). Parsa has many round exsolution features in and on the perimeter of olivine grains. Some linear exsolution features occur within the olivine grain (Figure 4.6). Between the streak and isolated blobs, an area describing most of the crystal, the olivine grains are void of inclusions. Parsa and Sahara 97096 are nearly equal in Cr_2O_3 content and therefore may have experienced a nearly equal degree of thermal metamorphism. Like Sahara 97096, Parsa exsolution features streak across olivine grains. Distinct from Sahara 97096, Parsa exhibits large exsolution blobs, $\sim$4.0μm, found in the center of olivine grains. Furthermore there are no exsolution features on the perimeter of the grain that complement the shape of the olivine grain as seen in Sahara 97096 (Figure 4.5 and 4.6). In comparing Sahara 97096 and Parsa, two samples with similar Cr_2O_3 content, we see at this degree of thermal metamorphism of olivine grains have exsolution streaks and the largest exsolution blobs measure greater than 1.0μm.

Kota Kota has the fourth most Cr_2O_3 with 0.200 wt%, the least amount of FeO 0.360 wt% and a high standard deviation of Cr_2O_3, 0.100 wt% (Table 4.1 and Figure 4.10). Kota Kota has exsolution features in and around olivine grains. Most of the grain is cluttered with exsolution features. Streaks can no longer be distinguished when observed with magnifications much less than 800x because little space between exsolution blobs exists (Figure 4.7). At 2,500x exsolution features are linear (Figure 4.9). Exsolution features on the perimeter of the olivine grain complement the shape of the olivine grain, extend around half the olivine grain perimeter, and are as large as $\sim$20.0μm. Kota Kota experienced more thermal metamorphism than Yamato 691, Sahara 97096, and Parsa. At this degree of thermal metamorphism exsolution features dominate the area within and around the crystal structure. Streaks are obscured by the abundance of exsolution features at magnitudes greater than 2,500x. Exsolution features border up to 50% of the olivine grain perimeter.

Qingzhen contains the least amount of Cr_2O_3, with 0.056 wt% and the lowest standard deviation of Cr_2O_3, with 0.056 wt% (Table 4.1 and Figure 4.10). Exsolution features are seen in and around olivine grains (Figure 4.8). At a magnitude of 2,030x no streaks are visible. On the perimeter of the olivine grain exsolution blobs

are as big as 5.2μm. Between exsolution blobs, an area describing most of the crystal, olivine grains are void of exsolution features. Of the five samples Qingzhen has experienced the highest degree of metamorphism. Isolated exsolution blobs, large and small, remain in and around olivine depleted in minor elements.

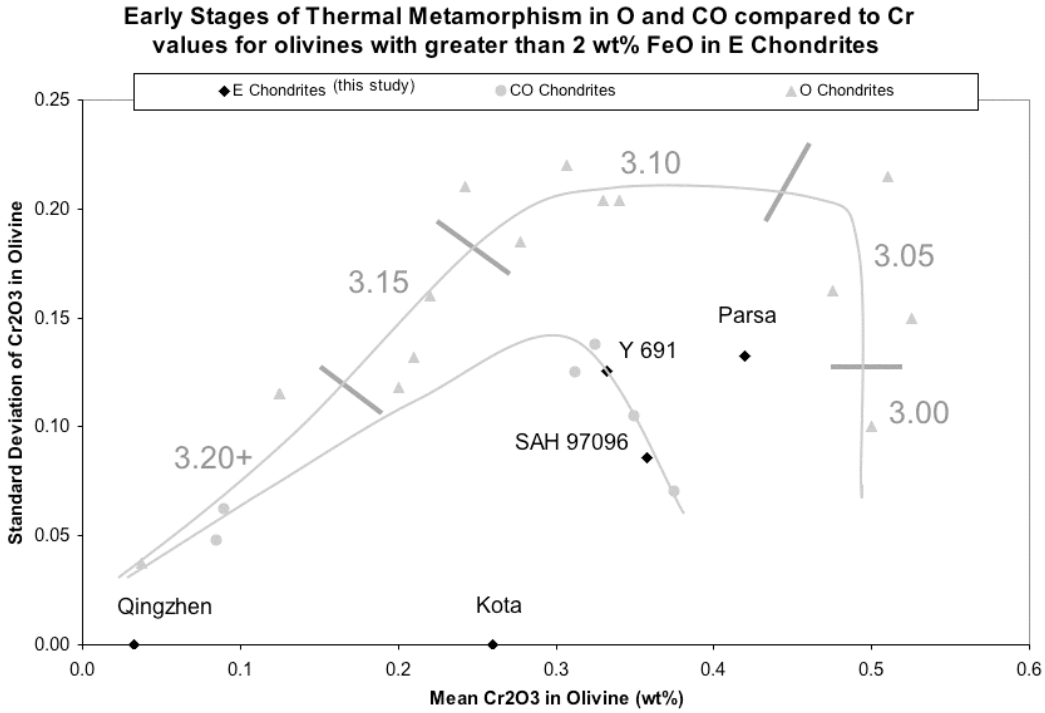

Figure 5.2: Early stages of thermal metamorphism in O and CO compared to Cr values for olivines with greater than 2 wt% FeO in E chondrites

If this study had only look at olivine with more than 2 wt% FeO, the data set would have been dramatically reduced. When graphing the Cr_2O_3 values for olivines with greater than 2 wt% FeO (Figure 5.2) Parsa, Yamato, and Sahara 97096 all plot further right

(Figure 5.1). Kota Kota and Qingzhen would each have only one data point and would hence plot on the x-axis. The data of only olivine grains with more than 2 wt% do not show a definite trend (Figure 5.2). With only three data points a trend could be interpolated beginning at Parsa and trending through the Yamato 691 and Sahara 97096 data points. As seen in the results Cr_2O_3 in olivine with less than 2 wt% FeO in E chondrites indicate metamorphism. Hence it is unnecessary to consider only olivines with greater than 2 wt% FeO. Furthermore we see that in considering only olivines with greater than 2 wt% FeO greatly reduces the amount of data.

Pristine olivine contains minor elements. When exposed to heat, minor elements exsolve out of the olivine crystal structure. This is true for olivine in O, CO, and E chondrites. Hence the E chondrite trend parallels the O and CO trends. Therefore the E chondrite Yamato 691, which contains olivine with the highest mean Cr_2O_3 wt%, is the most primitive. Following this trend the E chondrites in the study are ordered from most to least primitive: Yamato 691, Sahara 97096, Parsa, Kota Kota, Qingzhen.

These meteorites describe a trend and therefore are representations of different stages in the onset of thermal metamorphism. The most primitive meteorite Yamato 691 shows that at the initial stages of thermal metamorphism generate linear exsolution

features within the olivine grains. Exsolution is absent on the perimeter of olivine grain. Both Sahara 97096 and Parsa, which show a higher degree of thermal metamorphism, have exsolution streaks within the olivine grain and possibly on the perimeter of the olivine grain. The largest exsolution blobs measure greater than 1.0μm. At a higher degree of thermal metamorphism exsolution features dominate the area within and around the crystal structure. Streaks are obscured by the abundance of exsolution features at magnitudes greater than 2,500x. Exsolution features border up to 50% of the olivine grain perimeter. Qingzhen describes the most thermally metamorphosed phase. Little is left to measure. Isolated exsolution blobs, large and small, remain in and around olivine depleted in minor elements.

If one wanted to learn about EH chondrites in the early solar system they would study Yamato 691 since it is the most pristine of the five samples. This study extends the Grossman and Brearley (2005) method to E chondrites. It is a straight forward method that identifies the most primitive meteorites.

CHAPTER 6

CONCLUSION

E chondrites are important because they are the only chondrites to have an oxygen isotopic composition similar to that of the Earth and Moon and thus may be analog material from which the Earth formed. To identify which EH chondrites have been the least metamorphosed since formation is to find the EH chondrites that contain the most information about the early Solar System. This is the first study to look at the onset of thermal metamorphism in EH chondrites to identify the most pristine EH chondrite. The purpose of this study is to understand the redistribution of Cr during thermal metamorphism and to determine if results for EH chondrites found with Grossman and Brearley's (2005) method,

using olivine as an indicator of thermal metamorphism, can be applied to EH3 chondrites.

During thermal metamorphism Cr is redistributed into metal and sulfide phases, called exsolution features, in and around olivine grains. During the initial stages of heating, thermal metamorphism generates linear exsolution features within the olivine grains. Constituents within the linear exsolution features are on the order of $\sim$0.20μm. Increased heating causes the constituents within the linear exsolution features to increase in size, olivine grains to exhibit exsolution streaks, and possibly exsolution features on the perimeter of the olivine grain. The largest exsolution blobs measure greater than 1.0μm. With even more heating, exsolution features dominate the area within and around the crystal structure. Streaks are obscured by the abundance of exsolution features at magnitudes greater than 2,500x. Exsolution features border up to half of the olivine grain perimeter. Even more heating isolates exsolution blobs, large and small, which remain in and around olivine depleted in minor elements.

The streaks are nearly linear patterns suggesting structural control on the exsolution process. Crystal faces may provide zones of weakness that are easier to exsolve along. Larger exsolution features grow around the circumference of an olivine grain possibly

because a larger zone of weakness exists between the olivine and adjacent enstatite crystals.

This study finds it valid to apply the Grossman and Brearley (2005) method to EH3 chondrites. In this study of EH3 chondrites non-relationships between minor elements and FeO indicate that the redistribution of Cr is due to metamorphism and not volatility.

Distinctive exsolution features characteristic for varying amounts of heat, thermal metamorphism, makes Cr in olivine is a good indicator of the early onset of thermal metamorphism in E chondrites. Hence olivine in E chondrites, more specifically exsolution features and elemental abundances, can be used to find the most primitive E chondrites. This study found the petrological types of five E chondrites, ordered from most to least primitive, they are: Yamato 691, Sahara 97096, Parsa, Kota Kota, Qingzhen. If one wanted to learn about EH chondrites in the early solar system they would study Yamato 691 since it is the most pristine of the five samples. This study determined the degree of thermal metamorphism in five EH chondrites relative to one another. More samples for further study are needed to determine the petrologic type of each EH chondrite.

BIBLIOGRAPHY

Ashworth, J. R.: 1979, *Mineralogical Magazine* **43**, 535

Bhandari, N., Gopalan, K., and Rao, M. N.: 1975, *Meteoritics and Planetary Science* **10**, 362

Chizmadia, L. J., Rubin, A. E., and Wasson, J. T.: 2002, *Meteoritic and Planetary Science* **38**, 1781

Dehart, J. M., Lofgren, G. E., Lu, J., Benoit, P. H., and Sears, D. W.: 1992, *Geochimica Cosmochimica Acta* **56**, 3791

Dodd, R. T.: 1973, *Contributions to Mineralogy and Petrology* **42**, 159

Grevesse, N. and Sauval, A. J.: 1998, *Space Sci. Rev.* **85**, 161

Grossman, J. N. and Brearly, A. J.: 2005, *Meteoritics and Planetary Science* **40(1)**, 87

Hutchinson, R.: 2004, *Meteorites: a petrological, chemical and isotopic synthesis*, Cambridge University Press, The Edinburgh Building, Cambridge, CB2 2RU, UK

Johnson, C. A. and Prinz, M.: 1991, *Geochimica Cosmochimica Acta* **55**, 893

Jones, R. H. and Lofgren, G. E.: 1993, *Meteoritics* **28**, 213

Keil, K.: 1968, *Journal of Geophysics* **73**, 6945

Landstreet, J. D.: 2003, *Physical Processes in the Solar System*, Keenan and Darlington, Publishers, London, Ontario, Canada

Leitch, C. A. and Smith, J. V.: 1982, *Geochemica et Cosmochimica Acta* **46**, 2083

McCoy, T. J., Scott, E. R., Jones, R. H., Keil, K., and Taylor, G. J.: 1991, *Geochimica Cosmochimica Acta* **55**, 601

McSween Jr., H. Y.: 2000, *Meteorites and Their Parents Planets*, Cambridge University Press, Cambridge, United Kingdom

Scott, E. R. and Jones, J. N.: 1990, *Geochimica Cosmochimica Acta* **54**, 2485

Sears, D. W., Batchelor, J. D., Lu, J., and Keck, B. D.: 1991, *Proceedings of the NIPR Symposium on Antarctic Meteorites* **4**, 319

Sears, D. W., Grossman, J. N., Melcher, C. L., Ross, L. M., and Mills, A. A.: 1980, *Nature* **287**, 791

Shima, M., Shima, M., and Hinterberger, H.: 1973, *Earth and Planetary Science Letters* **19(2)**, 246

Sutton, S. R., Bajt, S., and Jones, R.: 1996, *Lunar and Planetary Science XXVII* **27**, 1291

Van Schums, W. R. and Wood, J. A.: 1967, *Geochimica Cosmochimica Acta* **31**, 747

Wang, D. and Xie, X.: 1997, *Geochimica Cosmochimica Acta* **4**, 277

Wasson, J. T.: 1985, *Meteorites: their record of early solar-system history*, W.H. Freeman and Company, New York, United States of America

Weisberg, M. K., Kimura, M., McCoy, T. J., and Lin, Y.: 2005, pp 1260–1261, Lunar and Planetary Sciences

Weisberg, M. K., McCoy, T. J., and Krot, A. N.: 2006, in D. Lauretta and E. H.Y. McSween (eds.), *Meteorites And The Early Solar System II*, pp 19–52, The University of Arizona Press

Weisberg, M. K. and Prinz, M.: 1998, p. 1741, Lunar and Planetary Sciences

Weisberg, M. K., Prinz, M., and Fogel, R. A.: 1994, *Meteoritics* **29**, 362